



Single-Cell Mapping of Brain Myeloid Cell Subsets Reveals Key Transcriptomic Changes Favoring Neuroplasticity after Ischemic Stroke

Fangxi Liu¹ · Xi Cheng² · Chuansheng Zhao^{1,3} · Xiaoqian Zhang¹ · Chang Liu³ · Shanshan Zhong¹ · Zhouyang Liu¹ · Xinyu Lin¹ · Wei Qiu² · Xiuchun Zhang¹

Received: 16 November 2022 / Accepted: 27 May 2023 / Published online: 27 September 2023

© Center for Excellence in Brain Science and Intelligence Technology, Chinese Academy of Sciences 2023

Abstract Interactions between brain-resident and peripheral infiltrated immune cells are thought to contribute to neuroplasticity after cerebral ischemia. However, conventional bulk sequencing makes it challenging to depict this complex immune network. Using single-cell RNA sequencing, we mapped compositional and transcriptional features of peri-infarct immune cells. Microglia were the predominant cell type in the peri-infarct region, displaying a more diverse activation pattern than the typical pro- and anti-inflammatory state, with axon tract-associated microglia (ATMs) being associated with neuronal regeneration. Trajectory inference suggested that infiltrated monocyte-derived macrophages (MDMs) exhibited a gradual fate trajectory transition to activated MDMs. Inter-cellular crosstalk between MDMs and microglia orchestrated anti-inflammatory and repair-promoting microglia phenotypes and promoted post-stroke neurogenesis, with SOX2 and related Akt/CREB signaling as the underlying mechanisms. This description of the brain's immune landscape and its

relationship with neurogenesis provides new insight into promoting neural repair by regulating neuroinflammatory responses.

Keywords Ischemic stroke · Monocyte-derived macrophage · Microglia · Neurogenesis · Single-cell sequencing

Introduction

Immune responses triggered by cerebral ischemic injury are often initiated by microglial activation in the peri-infarct area [1]. Peripheral immune cells then infiltrate the ischemic brain through the compromised blood-brain barrier and collaborate with brain-resident immune cells to elicit a long-lasting immune response [2]. Therefore, understanding the peri-infarct immune microenvironment may provide new perspectives to promote post-stroke brain repair. Preliminary studies have shown that resident and infiltrating immune cells in the brain perform different functions at different stages after stroke [3, 4]. Studies analyzing bulk cell populations have suggested the existence of potential immunological communications between brain-resident and infiltrated peripheral cells that contribute to neuronal injury, protection, or repair in the ischemic brain [5, 6]. However, direct evidence is still needed to further clarify the intricate immunological network in the peri-infarct area. Single-cell transcriptomic techniques are suitable for revealing cellular heterogeneity, and they have been applied in mapping the single-cell atlas of the homeostatic brain and identifying disease-related immune cells in multiple sclerosis and Alzheimer's disease [7–10]. Upon entering the ischemic brain, peripherally derived cells undergo

Fangxi Liu and Xi Cheng contributed equally to this work.

Supplementary Information The online version contains supplementary material available at <https://doi.org/10.1007/s12264-023-01109-7>.

✉ Wei Qiu
qiuwei@mail.sysu.edu.cn

✉ Xiuchun Zhang
15204090196@163.com

¹ Department of Neurology, The First Affiliated Hospital of China Medical University, Shenyang 110001, China

² Department of Neurology, The Third Affiliated Hospital of Sun Yat-sen University, Guangzhou 510630, China

³ Stroke Center, The First Affiliated Hospital of China Medical University, Shenyang 110001, China

genomic reprogramming or exhibit expression patterns similar to those of resident brain cells [11]. This suggests that the conventional bulk-sequencing method may fail to identify some types of cells and lose transcriptomic information. Consequently, high-resolution single-cell RNA sequencing can be applied to more accurately depict peri-infarct immune cells and elucidate their roles in the repair process.

Here, we first identified distinct cell clusters and their functions in the peri-infarct region, and then analyzed differentially-expressed genes under different conditions, with a focus on monocyte-derived cells (MDMs) and microglia. We then inferred the developmental trajectory of MDMs by using pseudo-temporal analysis and predicted the interactions between MDMs and brain-resident cells. Finally, we transferred bone marrow-derived MDMs to rats with stroke to further reveal their regulatory functions in neuroinflammatory responses and neuronal regeneration. Our results provide a single-cell atlas of peri-infarct cells and further demonstrate the role of MDMs and microglia in neuronal regeneration at single-cell resolution.

Material and Methods

Animal Preparation

Adult Wistar rats (male, 250–280g) were obtained from Beijing Weitonglihua Biotechnology Co. Ltd (Beijing, China). Experimental procedures were conducted in accordance with the Institutional Animal Care and Use Committee of China Medical University [SYXX [9] 2013-0007]. All rats were kept in rooms with 12-h circadian cycles and were given free access to food and water. Rats were randomly divided into four groups: (1) sham group (SHAM, $n = 23$); (2) ischemic group (ISC, $n = 23$); (3) ischemic group with bone marrow cell transplantation on postoperative day 3 (BMTC, $n = 23$); and (4) ischemic group with si-CCR2 Adeno-associated virus (AAV) treatment directly after establishment of the stroke model (si-CCR2, $n = 20$). Six rats in each group were sacrificed on day 14 for western blot and RT-qPCR analysis. Three rats in each group were sacrificed on day 14 for flow cytometry analysis of microglial polarization. Three rats in each group were sacrificed on day 3 for flow cytometry analysis of monocyte infiltration. Eight rats in each group were sacrificed on day 14 for immunofluorescence analysis. Three rats in the SHAM, ISC, and BMTC groups were sacrificed on day 14 for single-cell sequencing. Rats sacrificed on day 14 in each group were included in behavioral tests.

Rat Cerebral Ischemia Model and Stereotaxic Injection

Rats were anesthetized with isoflurane, induction with 4.5% isoflurane, and maintenance with 2% isoflurane. The rat stroke model was induced by stereotaxic injection of ET-1 (endothelin-1) (Sigma, USA) at the following coordinates (in mm): (1) anteroposterior (AP) +0.7, mediolateral (ML) +2.2, dorsoventral (DV) –2.0; (2) AP +2.3, ML +2.5, DV –2.3; and (3) AP +0.7, ML +3.8, DV –5.8. Each rat received 2 μ L ET-1 at each site at a rate of 0.5 μ L/min. The microsyringe was left *in situ* for 3 min after each injection. Lidocaine was applied to relieve postoperative pain. Rats were placed under a heating lamp until recovery from anesthesia. When the rats were lifted upside down by the tail, the right upper limb flexed toward the chest or tipped to the right during walking for ~24 h, indicating the successful establishment of the cerebral ischemia model. The mortality rate of ischemic rats was 30%.

AAVs were diluted to a concentration of 1.24×10^{12} viral genomes/mL and injected at a rate of 0.2 μ L/min into the peri-infarct area directly after the establishment of the stroke model. AAVs were injected at the following coordinates (in mm): (1) AP +1.5, ML 0, DV –2.0; (2) AP +1.4, ML +2, DV –2; and (3) AP +3, ML +2, DV –2. Each rat received a total of 3 μ L AAV. Efforts were made to minimize animal suffering and the number of animals used.

Behavioral Assessment

Rats received pre-training for 3 days prior to stroke model induction and neurological behavioral assessments were made on days 12–14 after ischemia, using the tapered/ledged beam-walking test, cylinder test, and sticky label test as previously described [12]. Experimenters responsible for video recording and behavioral evaluation were all blinded to the treatment group of rats.

On days 12–14 after cerebral ischemia, motor function was evaluated by the tapered/ledged beam-walking test. The beam consisted of two layers of trapezoidal planks, the upper layer narrower and the lower layer wider. The rats walked from the wide end to the narrow end, and the whole process was recorded by video. If the fore paw or rear paw completely fell on the lower trapezoidal board, it was recorded as a wrong step; if the paw landed on the edge of a narrow plank, it was recorded as a half wrong step. Slip ratio was calculated by the following formula: Slip ratio = (slip steps \div total steps) $\times 100\%$. A higher rate of slip steps indicated more serious impairment of limb motor function.

On days 12–14 after ischemia surgery, each rat was placed in a clear glass cylinder 20 cm in diameter and 50 cm high. The rats' activities in the cylinder were recorded for 3 min. The contact times between the forepaw and cylinder wall were calculated. The asymmetrical score of

forelimb use = [(use of impaired forelimb + 0.5 × use of both forelimbs) ÷ (total contacts)] × 100%. The higher the asymmetric score, the more severely impaired the forelimb motor function.

The sticky label test is often used to evaluate the sensorimotor function of the forelimb in rats. From days 12 to 14 after surgery, two 8 mm × 8 mm adhesive labels were affixed to the hairless area of the forepaws. The rats were quickly placed in a cage with a mirror and recorded with a camera for 2 min. The time of label contact and removal from both forepaws was recorded. If the rats could not tear off the sticky label within 2 min, the measure was eliminated.

Immunofluorescence

Deeply anesthetized rats received 4% PFA transcardially before their brains were harvested. The brains were cut into 8 μm sections for immunofluorescence staining. Every sixth section between bregma levels +0.7 mm and +2.3 mm was selected; six sections per rat were selected by a blinded researcher for quantification. Sections were incubated with primary antibodies against doublecortin (DCX), 5-ethynyl-2'-deoxyuridine (EdU), inducible nitric oxide synthase (iNOS), CD206/MRC1 (Mannose receptor, C type 1), CCR2 (C-C motif chemokine receptor 2) and Iba-1 (Allograft inflammatory factor 1) (Abcam, USA) at 4°C overnight. Then sections were incubated in a secondary antibody at room temperature and nuclei were stained with DAPI. Images were acquired using a confocal microscope (Olympus FV-1000, Japan). The mean integrated optical density (IOD) was measured with ImageJ and Fiji software. Sections with secondary antibody only, without primary antibody, were selected as negative controls.

Western blot

Protein was extracted from brain samples using lysis buffer containing protease inhibitors. Protein concentration was measured using a BCA reagent kit (Beyotime, China). Protein samples were mixed with SDS-PAGE loading buffer and boiled for 10 min. Samples were resolved onto 7%–12% gradient SDS-PAGE gels and then transferred electronically to polyvinylidene difluoride (PVDF) membranes. Afterward, the PVDF membranes were blocked with 5% non-fat milk and incubated with primary antibodies at 4°C overnight and then incubated with the secondary antibody for 2 h at room temperature. The protein bands were detected using the enhanced chemiluminescence (ECL) reagent kit (Thermo, USA).

Bone Marrow-derived Macrophage Culture and Adoptive Transfer

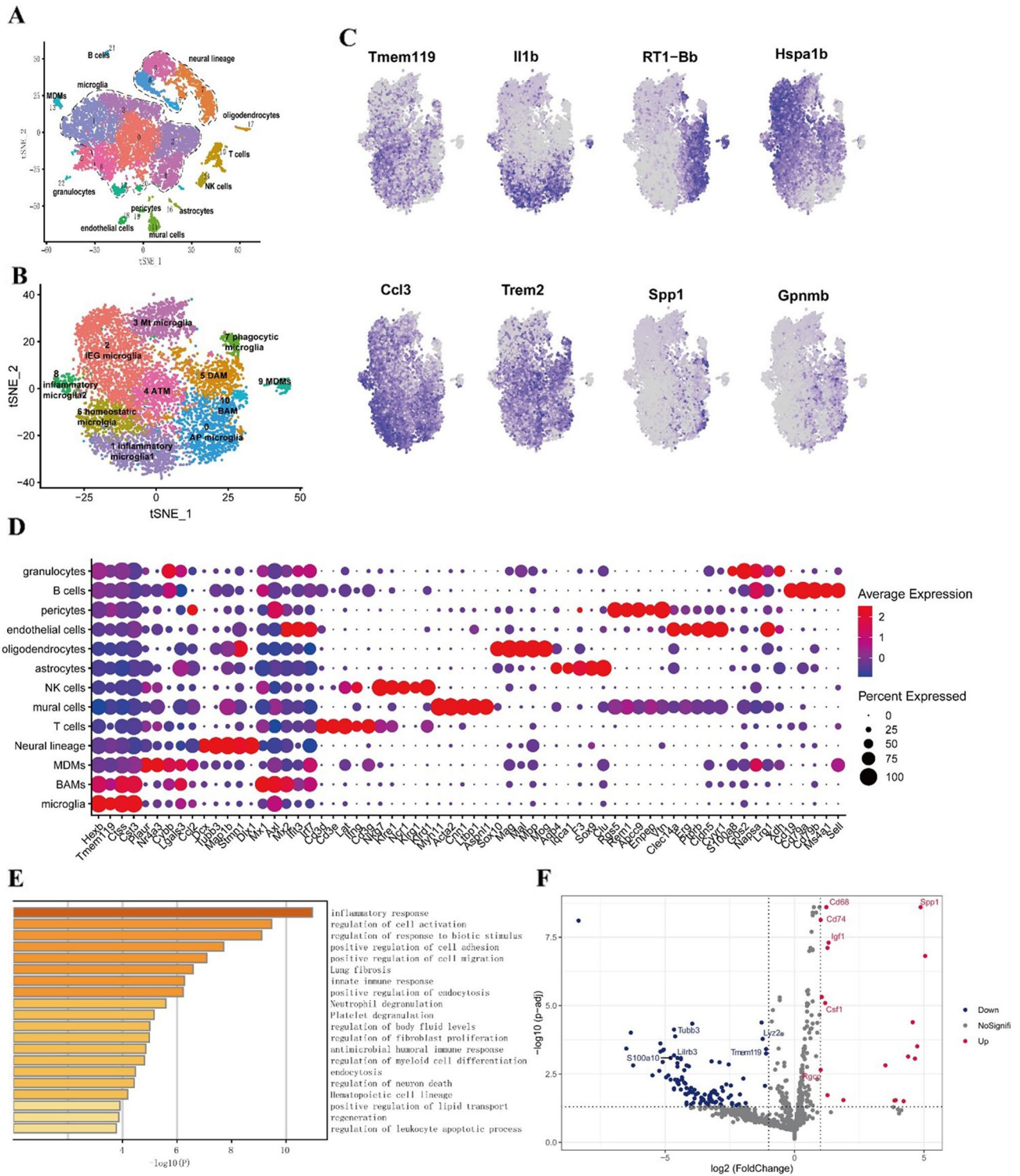
Femoral bones were collected from adult rats and bone marrow cells were obtained by flushing out cells from femoral bone cavities. After filtering through a cell strainer, bone marrow cells were treated with ACK lysis buffer (Solarbio, China) to remove red blood cells. Then bone marrow cells were cultured at 37°C and 5% CO₂ in RPMI medium containing 10% FBS (Biological Industries, Israel), 1% Penicillin-Streptomycin Liquid (Solarbio, China), and 10 ng/mL murine macrophage-colony stimulating factor (M-CSF) (PeproTech, USA) in low-attachment surface plates. Cells were cultured for 3 days and then collected for adoptive transfer. We transplanted bone marrow macrophages on post-operative day 3 by tail vein injection and each rat received 10⁶ cells in 1 mL PBS.

Flow Cytometric Analysis

Brains tissue was digested in RPMI medium containing 2 mg/mL collagenase II (Sigma) and 100 ng/mL DNase I (Sigma) at 37°C for 45 min, and then a 2-fold volume of RPMI medium containing 10% FBS was added to stop the digestion process. Cells were filtered and separated using a discontinuous Percoll (GE Healthcare) gradient (30% / 70%). We then used the isolated cells for staining. Cells were washed twice with cold PBS, resuspended with 100 μL 1× binding buffer and incubated with antibodies for 15 min at 25°C. This was followed by the addition of a binding buffer (400 μL) to collect data on a BD LSRFortessa flow cytometer (BD Bioscience, USA), and the data were analyzed using FlowJo 10 software (BD Pharmingen). Antibodies used in the study were rat anti-CD45-BV510, anti-CD11b-APC, anti-CD86-FITC, anti-CD163-PE, and anti-Ly6c-FITC. Representative gating strategies in flow cytometry analysis were CD11b^{hi}CD45^{hi} for MDM subtypes, CD11b⁺ CD45⁺ for microglia, and CD45^{low}CD11b^{med} for T cells.

Single-cell RNA Sequencing

We collected brain tissue immediately adjacent to the infarct core with a width of 2 mm peri-infarct from 3 rats and mixed them as one sample for each group. Single-cell suspensions of peri-infarct brain tissue were obtained as described above and special attention was paid to the 10× Genomics cell preparation guidelines. After cell debris clearance and quality control, single-cell sequencing was performed according to the 10× Genomics Chromium Single Cell 3' Reagent v3 Chemistry sequencing protocols (<https://support.10xgenomics.com>). Peri-infarct brain cells were first packed with gel beads [containing a sequencing primer binding site, a 16–base pair (bp) 10× barcode, a



10 bp UMI and a 30 bp poly-dT primer sequence] and reaction reagents, in order to form Gel beads in emulsion. Then after cell lysis, reverse transcription, and cDNA amplification, a transcriptional library was constructed for high-throughput sequencing. The depth of sequencing in the SHAM, ISC, and ISCBMMC groups was 55566 reads,

90374 reads, and 58568 reads per cell, respectively. Output sequencing data were aligned to the reference transcriptome (*Rattus_norvegicus_6.0*); feature-barcode matrices and clustering and gene expression analysis were generated using Cell Ranger V3.0.1.

Fig. 1 Single-cell RNA sequencing reveals cellular diversity in post-stroke peri-infarct brain tissue. **A** t-SNE plot colored by cell type shows the separation of 12,784 single cells into 23 distinct clusters. **B** t-SNE plot colored by cell type showing the separation of myeloid cells into 10 distinct clusters. **C** t-SNE feature plot showing the distribution of the expression of marker genes for each microglial cluster. **D** Dot plot showing the expression levels of marker genes in each cellular lineage (dot size represents the percentage of cells in each cell type expressing given marker genes; dot color represents the expression level of each marker gene; red dots indicate a higher expression level, while blue dots represent a lower expression level). **E** Barplot showing statistically enriched terms of marker genes for axon tract-associated microglia. **F** Volcano plot showing the differentially-expressed genes ($P < 0.05$, $\log_2(\text{FC}) > 1$ or $\log_2(\text{FC}) < -1$) in axon tract-associated microglia between ISC and SHAM conditions (red dots represent significantly up-regulated genes, blue dots represent significantly down-regulated genes, grey dots represent non-significantly expressed genes). ATM, axon tract-associated microglia; DAM, disease-associated microglia; IEG MG, immediate early gene enriched microglia; Mt. MG, mitochondrial gene enriched microglia; AP microglia, antigen processing- and presentation-related microglia; MDMs, monocyte-derived macrophages; BAMs, border-associated macrophages.

Downstream Analysis of Single-cell Sequencing Data

After obtaining the expression matrices from Cell Ranger, we applied downstream analysis with R version 3.5.0. The first steps of downstream analysis were conducted by using the R package Seurat (v3.1.5). Cells with a count of features ranging from 400 to 4500, UMI count > 600 , and cells containing $< 10\%$ mitochondrial genes were included for downstream analysis. We found integration anchors using the first 20 dimensions and applied dataset integration (ISC-SHAM and ISCBMMC-ISC) using these anchors. The data were normalized and scaled with default parameters, then we applied PCA and used the first 30 principal components to reduce dimensions. Unsupervised shared nearest neighbor was applied with a resolution of 1 to cluster cells and t-SNE was selected for visualization. Finally, markers for each cluster were calculated with the “FindAllMarkers” function embedded in the R package Seurat using a log₂-fold-change in threshold of 0.25 and minimum pct of 0.1. Differentially expressed genes between conditions in certain microglia clusters were identified using the R package SCDE (v1.99.1) and the “FindMarker” function in Seurat.

Functional Enrichment Analysis

Functional enrichment analysis was applied using the online database Metascape. In Metascape enrichment analysis, terms with a P -value < 0.01 (calculated based on the cumulative hypergeometric distribution), a minimum count of 3, and an enrichment factor > 1.5 (calculated as observed counts/counts expected by chance) were collected and clustered based on membership similarities; q -values are P -values adjusted by Benjamini-Hochberg multi-test, and Kappa

scores are selected as the similarity metric when clustering enriched terms. Bar plots show the most statistically significant term within a cluster. In the network plot, terms with a similarity > 0.3 are considered as a cluster and connected by edges. We also calculated Z scores for statistically significant functional enrichment terms and presented them in bubble plots by using the GOplot R package (version 1.0.2).

Monocle Trajectory Inference

We used the R package Monocle (v2.10.1) to order cells in pseudotime and infer the trajectory of neural lineage cell development. First, we subsetted transcription data of clusters identified as the neural lineage from the Seurat object and created Monocle cds subjects from these clusters. After quality control and normalization, we clustered cells and applied a differential gene test to find genes distinguishing cell types. We selected the top 1000 of these genes according to their q -value to define a cell’s progress. Then we applied dimension reduction using the “DDRTree” method and ordered cells in a pseudotime trajectory. To cluster genes by pseudo-temporal expression pattern, we applied the differential gene test again with a formula string of pseudotime and plotted a heatmap of 3 clusters using genes with a q -value $< 10^{-4}$. To analyze branches in single cell trajectory, we applied the BEAM test and plotted a heatmap of 2 clusters using genes with a q -value $< 10^{-6}$.

Statistical Analysis

Statistical analysis was performed with GraphPad Prism 8. Data are presented as the mean \pm SEM, a P value < 0.05 was considered statistically significant, and the asterisks indicate significance: $*P < 0.05$, $**P < 0.01$, $***P < 0.001$. Normality tests were applied before one-way ANOVA parametric analysis. In the comparison of data from three groups, non-parametric tests were applied. The results were corrected for multiple comparisons using statistical hypothesis testing (Dunnett).

Results

scRNA-seq Reveals That Microglia Are the Major Cell Type in the Peri-infarct Area

We performed single-cell RNA sequencing analysis of peri-infarct and sham-operated brain tissue from rats on day 14 post-operation using the 10X Genomics Chromium platform. The t-distributed stochastic neighbor embedding projection in the R package Seurat [13] showed that the 12,784 cells from the combined dataset were separated into 23 distinct clusters (Fig. 1A, Table S1), and the origin of each cell

was also visualized (Fig. S1). The expression levels of well-characterized marker genes were then used to annotate these distinct cell-type clusters (Fig. 1D, Table S2). Microglia were identified as the predominant cell clusters in the peri-infarct region based on their expression of *Tmem119*, *Hexb*, *Ctss*, and *Cst3* (Fig. 1D) [7]. Adjacent to microglia was a separate cluster of brain-resident macrophages, namely central nervous system border-associated macrophages (BAMs), which showed higher expression of the BAM marker *Axl* [7], genes associated with antigen processing and presentation (e.g., *Cd74* and *RT1-Ba*), and the interferon-inducible GTP-binding proteins *Mx1* and *Mx2* (Fig. 1D, Fig. S4). However, the BAMs lacked expression of the microglial marker gene *Tmem119*. Another cluster of macrophages was identified as MDMs, which exhibited a greater expression of macrophage markers in PanglaoDB (*Nr4a3* and *Plaur*) [14] (Fig. 1D, Fig. S1E). MDMs also showed higher expression levels of antigen processing- and presentation-associated genes. Based on the expression of *Tubb3* and *Dcx*, the neural lineage, another major component of the peri-infarct cells, was then identified. Based on the transcriptional signatures of *Mki67*, *Ccnd2*, and *Stmn1*, neural lineage cells were further divided into four clusters (Fig. S1D). Furthermore, in addition to neuronal and microglia clusters, mural cells, T cells, B cells, myelinating oligodendrocytes, ependymal cells, pericytes, astrocytes, and granulocytes were also identified by their respective marker genes (Fig. 1D).

Diverse Gene Expression Patterns and Functional States of Microglia in the Ischemic Brain

To gain a deeper understanding of the heterogeneity of myeloid cell clusters, we re-clustered the subset of myeloid cells into 11 clusters based on marker genes identified by the R package Seurat (Fig. 1B, 1C).

Cells in cluster 6 were identified as homeostatic microglia based on the heightened expression of typical microglia marker genes *Hexb* and *Sparc* (Fig. S4). Adjacent to the homeostatic microglia was cluster 4, which shared similar transcriptomic features with ATMs (e.g., *Igf1*, *Spp1*, and *Gpnmb*) [15]. Enrichment analysis of marker genes for ATMs revealed their involvement in the biological processes neuronal regeneration and phagocytosis (Fig. 1E). To further elucidate the activation features of ATMs, we applied differential gene testing with the R package SCDE and found that antigen processing and presentation-related genes (*Cd74* and *RT1-A2*) and neuroregeneration-related genes (*Igf1*, *Spp1*, and *Gpnmb*) were upregulated. In contrast, microglia homeostatic state markers such as *Tmem119* were downregulated in the ischemic group compared to the sham counterparts (Fig. 1F, Table S3). Adjacent to ATMs, disease-associated microglia (DAMs, cluster 5) were identified based on their higher expression of *Spp1*, *Gpnmb*,

and antigen processing- and presentation-related genes [9]. Cluster 2 microglia (IEG microglia) were distinguished by higher expression of immediate early genes (*Hspa1b* and *Jun*). Adjacent to cluster 2 was cluster 3, which showed a higher expression of mitochondrial genes. Clusters 1 and 8 were characterized by high expression of inflammation-related genes (e.g., *Il1b*, *Ccl3*, and *Ccl4*). Marker genes of cluster 83 (e.g., *Gadd45b*) were identified as essential genes for p38 MAPK signaling, which is essential for microglia-mediated neuroinflammation (Fig. 1C, Fig. S4) [16]. In addition, single-cell sequencing identified a microglial cluster with high expression of phagocytosis-related genes such as *Trem2* (cluster 7) and a microglia cluster associated with antigen processing and presentation (AP microglia, cluster 0) (Fig. 1C, Fig. S4).

Transcriptomic Changes of Infiltrated Macrophages Following Cerebral Ischemia

Immune responses triggered by peripheral blood-infiltrated immune cells are critical regulators of post-stroke ischemic brain injury and repair. Therefore, we obtained an expression matrix of macrophages to identify single-cell-level transcriptomic changes in macrophages following a stroke. 203 genes were significantly upregulated, and 211 genes were significantly down-regulated ($P < 0.05$) in MDMs from ischemic brain tissue relative to sham-operated brain tissue, as determined by differential gene expression analysis (Fig. 2A, Table S4). Then Gene Ontology (GO) enrichment analysis revealed that the significantly upregulated differentially-expressed genes (DEGs) were predominantly associated with biological processes such as import into cells (*Psap* and *Prkcg*), innate immune response, cell adhesion (*Esam*), transmembrane receptor protein tyrosine kinase signaling pathway (e.g., *Cyfp2*, *Ptprf*, and *Runx2*), neural projection development (e.g., *Spp1* and *Nedd4*), and angiogenesis (e.g., *Plpp3*) (Fig. 2C, Table S5, S6). Significantly downregulated DEGs were mainly involved in antigen processing and presentation (*RT1-Ba* and *Fcgr1a*), immune regulatory interactions between a lymphoid and a non-lymphoid cell (*Cd83*, *Anxa1*, and *Icam2*), and inflammatory immune response (*Clec10a*, *Il1r2*, and *S100a6*) (Fig. 2D). Next, we conducted a pseudotime analysis of MDMs using the R package Monocle2 [17]. Pseudotime analysis showed that homeostatic MDMs from the SHAM group showed a developmental trajectory into MDMs from the ISC group (Fig. 2B). Enrichment analysis of pseudotime-dependent DEGs revealed associations with mRNA processing, macrophage markers, apoptotic process regulation, and cytokine production regulation (Fig. 3E Table S7, S8). TRRUST (Transcriptional Regulatory Relationships Unraveled by Sentence-based Text mining) analysis revealed that these pseudo-dependent

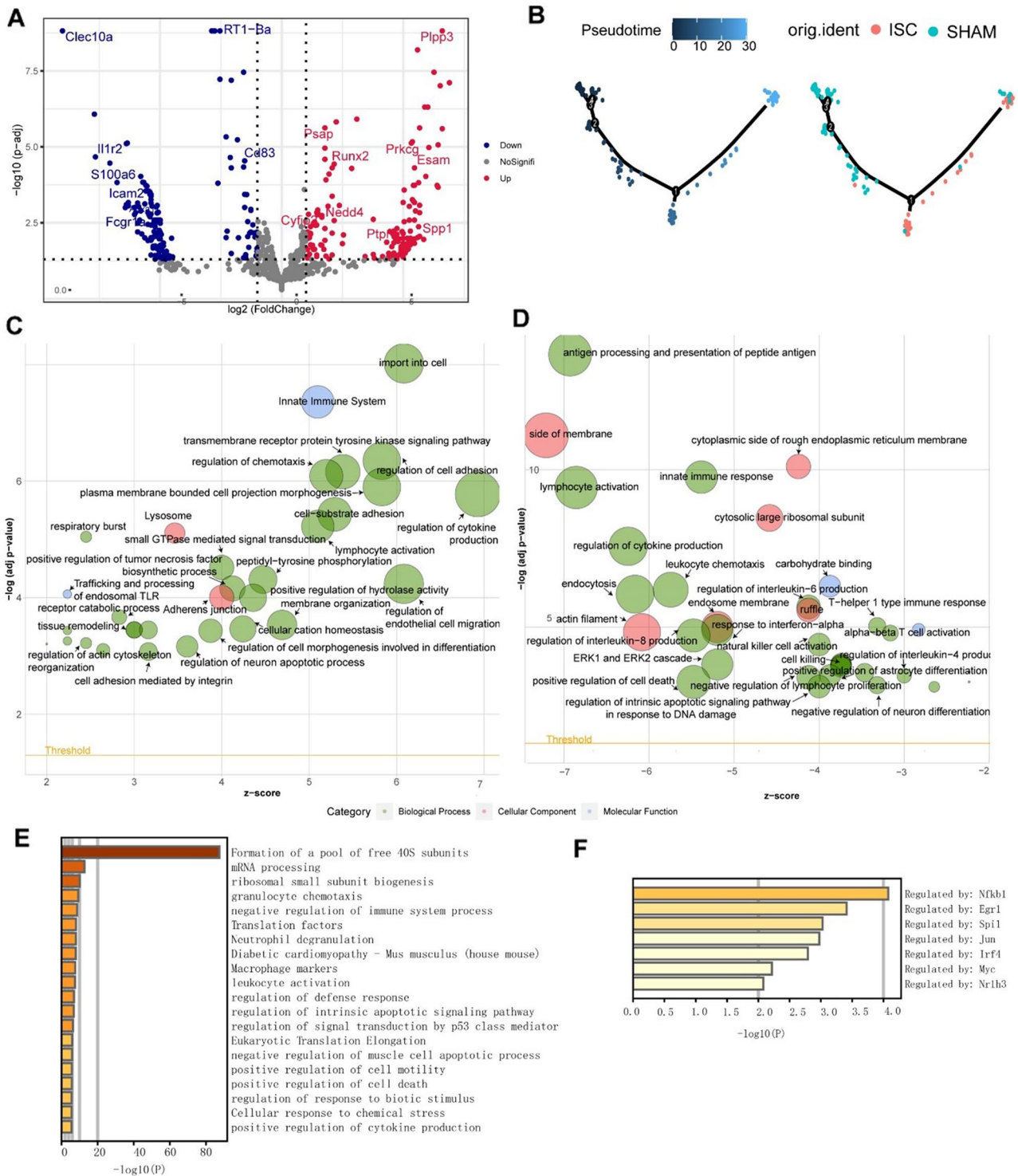


Fig. 2 MDMs show transcriptomic changes after infiltrating the ischemic brain. **A** Volcano plot showing the significantly differentially-expressed genes of MDMs between ISC and SHAM conditions ($P < 0.05$, $\log_2(\text{FC}) > 1$ or $\log_2(\text{FC}) < -1$ (red dots represent significantly up-regulated genes, blue dots represent significantly down-regulated genes, grey dots represent non-significantly expressed genes). **B** MDMs are positioned in a development trajectory constructed by Monocle and colored by pseudotime (left) or Seurat’s group identity (right) **C**, **D** Bubble plots showing the enriched GO terms of significantly up-regulated (**C**) or down-regulated (**D**) genes between ISC

and SHAM conditions. The threshold was set as Z-score > 2 or < -2 and $-\log(\text{adj } p\text{ value}) > 3$. The area of the displayed circles is proportional to the number of genes assigned to the term and the color corresponds to the category (green, biological processes; red, cellular components; blue, molecular functions). The complete gene and GO terms are listed in Supplementary Table 3. **E** Barplot showing the enrichment analysis of pseudodependent differentially-expressed genes. **F** Barplot showing the enrichment analysis of transcription factors of pseudodependent differentially-expressed genes in TRRUST.

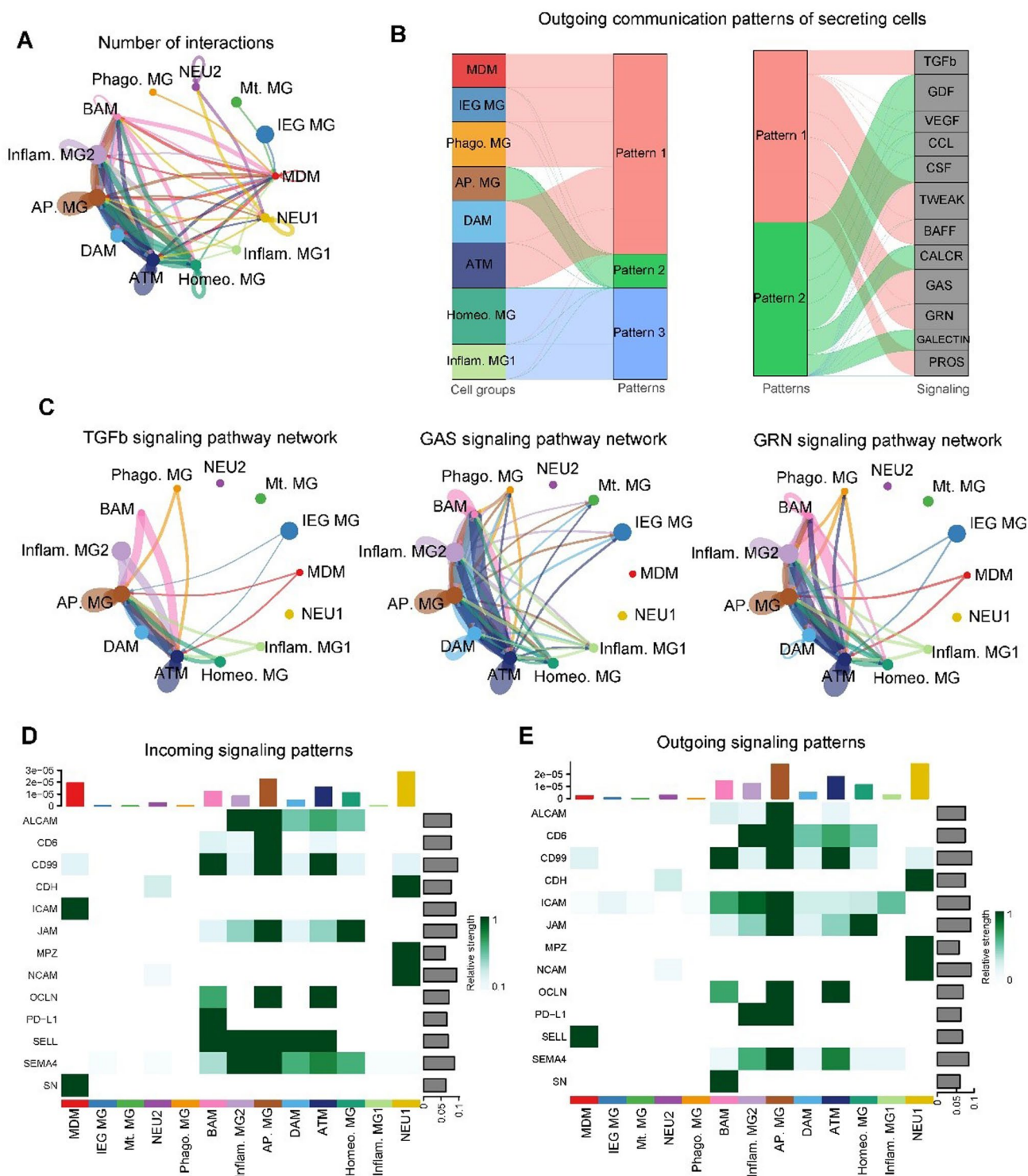


Fig. 3 Interactions between cells of myeloid and neural lineages. **A** Circle plot showing the number of interactions among cell clusters. Line thickness represents the number of interactions, the colors represent the cluster source of interactions. **B** River plot showing the global output communication patterns of secreting cells. **C** Circle plot visualization of the TGFb, GAS, and GRN signaling communication network using. **D**, **E** Heatmap showing input (**D**) and outgoing (**E**) signaling patterns in myeloid and neural lineages. The color

of each bar in the heatmap represents the relative strength of interactions. Phago. MG, phagocytic microglia; Mt. MG, mitochondrial gene-enriched microglia; IEG MG, immediate-early gene-enriched microglia; inflame. MG, inflammatory microglia; Homeo. MG, homeostatic microglia; ATM, axon tract-associated microglia; DAM, disease-associated microglia; AP. MG, antigen processing- and presentation-related microglia.

DEGs were primarily controlled by transcription factors *NFkb1*, *Jun*, and *Irf4* (Fig. 2F).

Interactions Between Myeloid Cell Populations and Cells of Neural Lineage

Next, we investigated intercellular interactions that may contribute to the different activation states and repair-promoting effects of peri-infarct cells in the ISC group. We focused our analysis on cells of the myeloid and neural lineages and used the R package CellChat to detect intercellular interactions [18]. CellChat detected 13 significant ligand-receptor pairs associated with cell-cell contacts and 18 secreted signaling ligand-receptor pairs (Fig. S5). Microglia showed more and stronger interactions with other cell types (Fig. 3A), suggesting an essential role for microglia in the microenvironment of peri-infarct brain tissue. We identified three patterns of output signaling in the global secreted communication network. A significant proportion of output secreted signals were mediated by myeloid cells and exhibited pattern #1 (Fig. 3B). Pattern #1 consisted primarily of the outgoing signaling of ATMs, immediate-early gene high microglia (IEG MGs), and monocyte-derived macrophages, representing pathways such as TGF β , TWEAK, BAFF, GAS, GRN, and PROS. Microglia, MDMs, and BAMs were all identified as sources of TGF β , GAS, and GRN signaling, with the primary targets being microglia and BAM populations in pattern #1 (Fig. 3B, C). In contrast, communication pattern #2 mainly included outgoing signals from inflammatory microglia (inflamm. MGs) that were mediated by GDF, VEGF, CCL, CSF, and galectin signaling (Fig. 3B, C). On the other hand, cells of the myeloid and neural lineages also showed communication through direct contact. MDMs interacted with microglia by secreting selectins, which may have contributed to their recruitment. Microglia were predicted to interact with neural lineage cells *via* the Sema pathway (Fig. 3D, E), which promotes neuronal generation [19].

Transplantation of BM-derived Macrophages Alters the Activation States of Peri-infarct Microglia

To further determine the function of infiltrated monocyte-derived cells, macrophages isolated from the bone marrow of homologous rats were transplanted intravenously. We injected 1 million macrophages derived from bone marrow into the tail veins of rats three days after a stroke, since monocyte infiltration peaks between days 3 and 4 [4]. We isolated peri-infarct brain tissue from rats transplanted with homologous macrophages and applied single-cell RNA sequencing analysis. Unsupervised graph-based clustering of 13,983 cells from the cell transplantation and ischemia groups presented a t-SNE plot of 26 clusters, with microglia also being the predominant cell type (Fig. 4A, S6, S7,

Table S9). Similar patterns of marker gene expression were found in the microglia of this combined dataset and the ISC-SHAM group, but the composition of each cluster was altered. Peri-infarct microglia were clustered into ATMs, IGE MGs, mitochondria gene-enriched microglia, homeostatic microglia, DAMs, phagocytic microglia, and inflammatory microglia. We found that the proportion of inflammatory microglia 1 and homeostatic microglia increased after bone marrow cell transplantation (Fig. 4B). Inflammatory microglia 1 was characterized by high expression of inflammatory cytokines (*Il1b* and *Ccl4*) and MAPK signaling-related genes (*Gadd45b* and *Nfkb1a*), and the expression levels of these marker genes were further increased in the BM-MC group compared to the ISC group. Homeostatic microglia were identified by their elevated expression of the homeostatic gene *Tmem119* and the MAPK/ERK signaling regulators *Tmem176a* and *Hspa1b* [20], which were upregulated in BM-MC microglia (Fig. 4C, D). Next, we sought to explore the DEGs in ATMs following bone marrow cell transplantation (Table S10). After bone marrow cell transplantation, ATMs (cluster1) showed upregulation of neuronal proliferation, differentiation-related *Igf1* and *Spp1* [21], antigen processing and presentation-related *RT1-Db1* and *RT1-Ba* and phagocytosis related *Axl* and *Gpnmb*. (Fig. 4E).

Next, we transplanted MDMs or injected si-CCR2 AAVs stereotaxically to increase or inhibit the infiltration of MDMs (Fig. S9). Our immunofluorescence results showed that bone marrow MDM transplantation significantly suppressed the expression of the pro-inflammatory microglial marker *iNOS* and increased the anti-inflammatory microglial marker *CD206* compared to the ISC group (Fig. S8C, D). Flow cytometry data showed that BMDM transplantation increased the proportion of CD163⁺ M2 microglia among all microglia (Fig. S8E, F).

BM-derived Macrophage Infiltration Favors Repair-promoting Transcriptomic Changes in the Neural Lineage

To characterize whether transcriptomic changes in bone marrow cells are associated with neurogenesis, we analyzed transcriptional data from neuronal cells and investigated the DEGs between the cell transplantation and the ischemic control groups. Differential expression tests revealed that transplanted bone marrow cells upregulated genes associated with neuronal stem cell differentiation (*Id4*), migration (*Tubb2a*), and axonal development (*Map1b*) (Fig. 5A, Table S11).

Next, we performed a pseudotime analysis of the neural lineage using Monocle. As depicted in the two-dimensional dendritic cell trajectory, the trajectory began with predominantly neuronal cells from cluster 8 (identified by the R

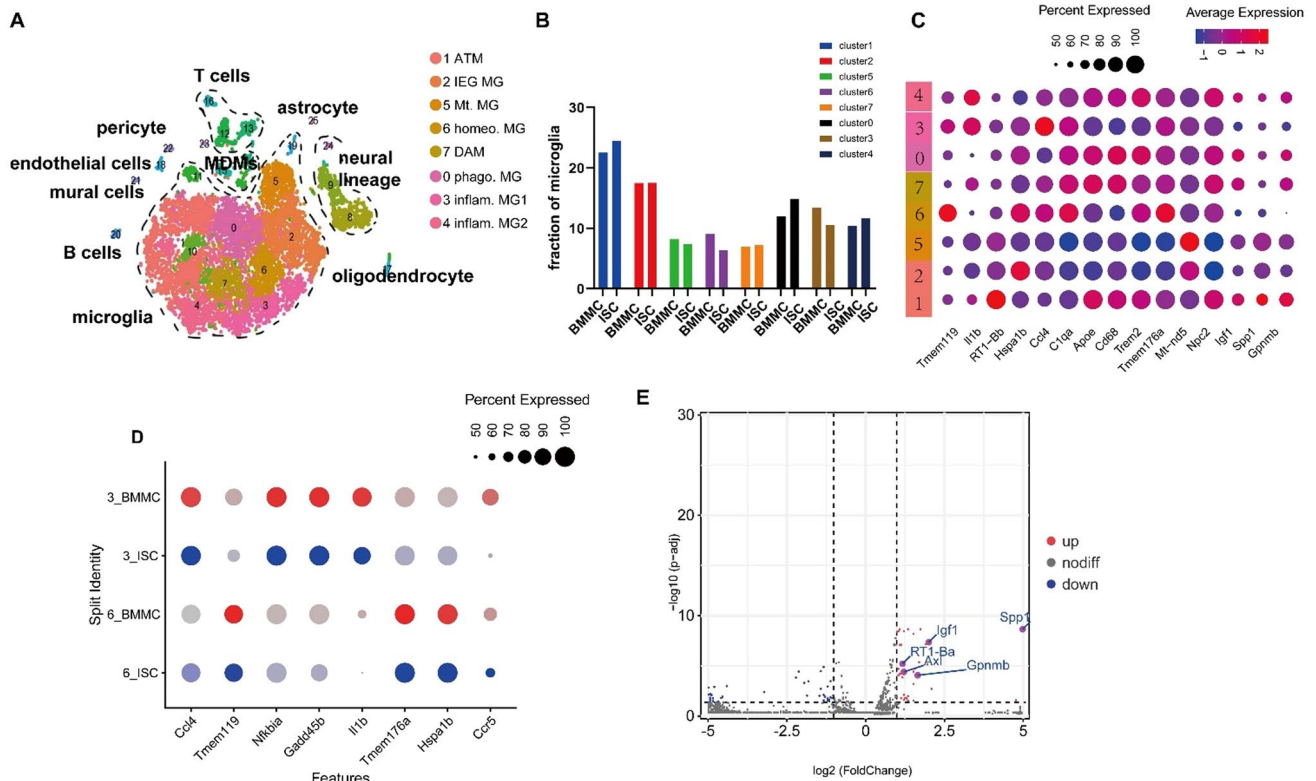


Fig. 4 Transplantation of bone marrow-derived monocytes alters the activation state of microglia. **A** t-SNE plot colored by cell type shows the integrated 13,983 cells from the BMMC and ISC group separate as 26 distinct cell clusters. **B** Bar plot showing the proportion of microglia from the BMMC or the ISC group. **C** Dots plot representing the expressed percentage and average expression level of selected marker genes for each microglial cluster. **D** Splitting dot plot showing the different expression levels and the percentage of cells expressing given marker genes in BMMC and ISC conditions (dot size, percent-

age of cells expressing given genes; red, higher expression; blue, lower expression). **E** Volcano plot showing significantly upregulated and downregulated genes (\log_2 fold change > 1 or < -1, $P < 0.05$) in ATMs from the BMMC group compared with the ISC group. ATM, axon tract-associated microglia; IEG MG, immediate-early gene-enriched microglia; Mt. MG, mitochondrial gene-enriched microglia; Homeo. MG, homeostatic microglia; DAM, disease-associated microglia; Phago. MG, phagocytic microglia; inflam. MG, inflammatory microglia.

package Seurat in the preceding section) (Fig. 5B). Then, close to the central node, neuronal cells began to exhibit a bidirectional trajectory. One trajectory branch (branch Y_83) was composed primarily of cluster 9 cells, while the other bifurcation (branch Y_23) was composed primarily of cluster 8 cells (Table S12). Branch analysis of pseudotemporal trajectories revealed that cells localized to cell fate 1 (corresponding to branch Y_83) were enriched for immune response-related genes (e.g., *ApoE*, *B2m*, *C3*, and *Ptprc*), myeloid cell activation (e.g., *Fcer1g* and *Trem2*), and phagocytosis (e.g., *C3* and *Aif1*) (Table S13). Upon the transition of pseudotime, these genes were initially upregulated and then downregulated (Fig. 5C–E). Meanwhile, genes involved in axonal development (e.g., *Ncam1* and *Map1b*), neuronal proliferation (e.g., *Cd24*), differentiation (e.g., *Dlx1*), and migration (e.g., *Dcx*) were upregulated with the transition to cell fate 2 (corresponding to branch Y_23) (Table S14). These genes also show pseudo-dependent upregulated expression (Fig. 5C, D, F).

Bone Marrow-derived Macrophage Transplantation Promotes Post-stroke Neurogenesis and Functional Recovery

To explore the regulators of neural regeneration after cell transplantation, we performed an enrichment analysis of pseudo-dependent upregulated genes in the neural lineage (Table S15). Our results showed they were involved in biological processes like translation regulation, cytoskeleton organization, positive neuron projection development regulation, and nerve growth factor response (Fig. 6A, Table S16). Next, using the Cytoscape plugin iRegulon [22], we investigated regulons and predicted potential transcription factors of pseudo-dependent upregulated genes. *Sox2* was the leading regulator of pseudo-dependent upregulated genes, including *Id4*, *Ncam1*, and *Dlx1*, as determined by an iRegulon analysis (Fig. 6B, S10, Table S17). *Sox2* also showed upregulation with pseudotime transition (Fig. S10).

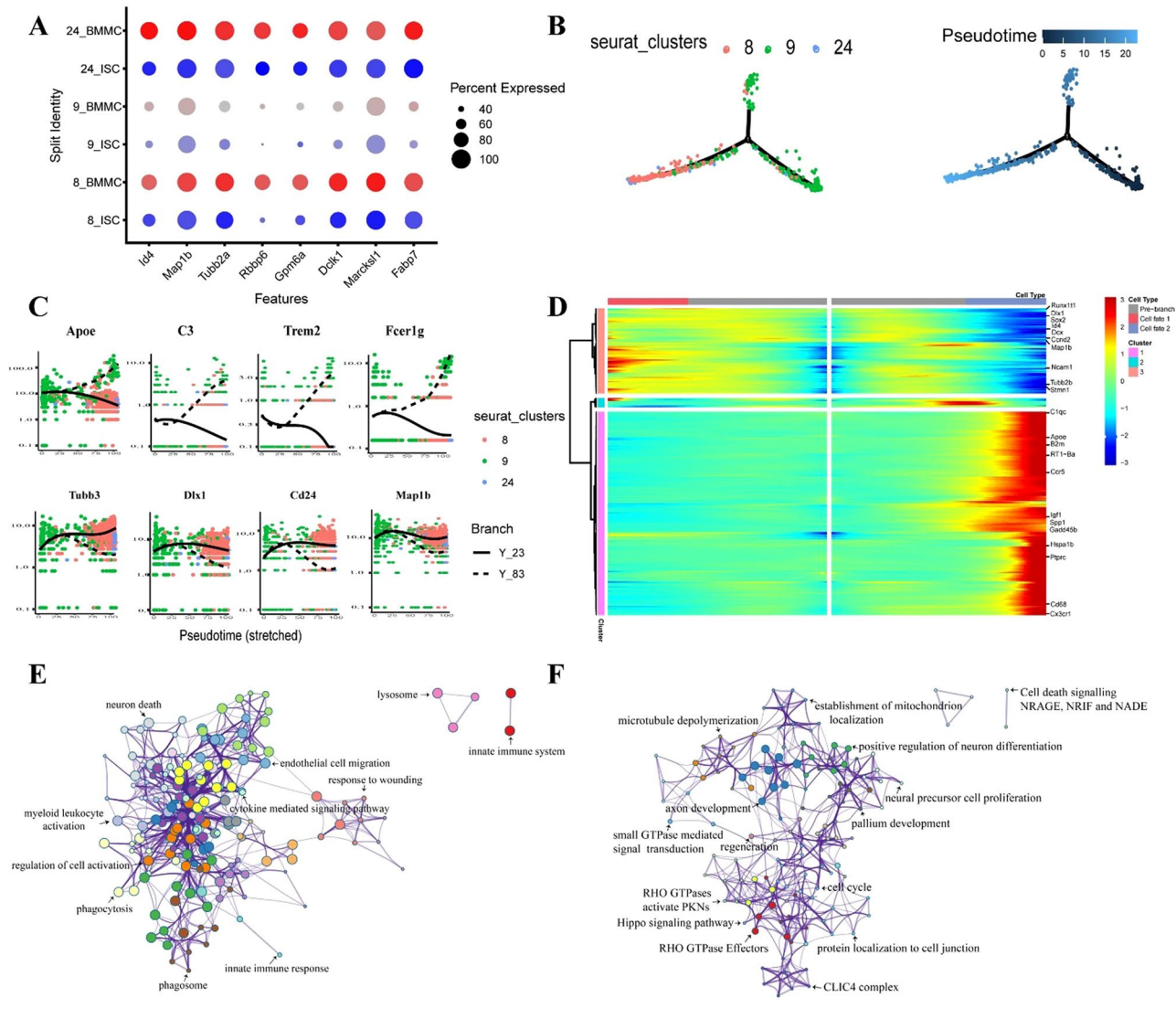


Fig. 5 Analysis of the neural lineage after transplantation of bone marrow-derived macrophages. **A** Dot plot comparing the expressed percentage and average expression level of Seurat-identified differentially-expressed genes between the BMMC and ISC groups in each cluster (dot size, the percentage of cells expressing given genes; red, higher expression; blue, lower expression). **B** Cells of neural lineage (clusters 8, 9, and 24) are positioned in a development trajectory constructed by Monocle and colored by Seurat cluster identity. **C** Dot

plots showing expression patterns of branch_Y83-dependent up-regulated genes (*Apoe*, *C3*, *Trem2*, and *Fcer1g*) and branch Y_23-dependent up-regulated genes (*Tubb3*, *Dlx1*, *Cd24*, and *Map1b*) according to pseudotime order, colored by Seurat's original cluster colors. **(D)** Heatmap showing the clustering of branch-dependent genes with a q -value $< 10^{-4}$ in the BEAM test, corresponding to cell fate transition. **E**, **F** Functional enrichment network of branch_Y83-dependent (**E**) and branch Y_23-dependent (**F**) up-regulated genes.

Next, we investigated the neurogenesis of the subependymal ventricular zone (SVZ) by treating rats with EdU and applying immunofluorescent staining to detect EdU and DCX-positive cells. Our results showed that bone marrow MDM transplantation increased the number of EdU-positive cells in the SVZ, while si-CCR2 AAV injection significantly decreased the number of DCX-positive cells in the SVZ (Fig. 6C, D). To evaluate functional recovery, the beam-walking test, sticky label test, and cylinder test were administered from postoperative day 12 to day 14. Rats in the si-CCR2 AAV injection group showed a significant

increase in forelimb slip rate in the beam-walking test and an increase in asymmetry score in the cylinder test (Fig. S8B).

Sox2 has been shown to promote neural progenitor cell differentiation [23]. *Sox2* is a transcriptional regulator of both Akt and CREB signaling, which are indispensable components of the pseudotime-dependent upregulated neurotrophin pathway. Western blotting analysis of the peri-infarct brain tissue showed that transplantation of bone marrow macrophages increased the expression levels of Akt and CREB signaling (Fig. 6E, F).

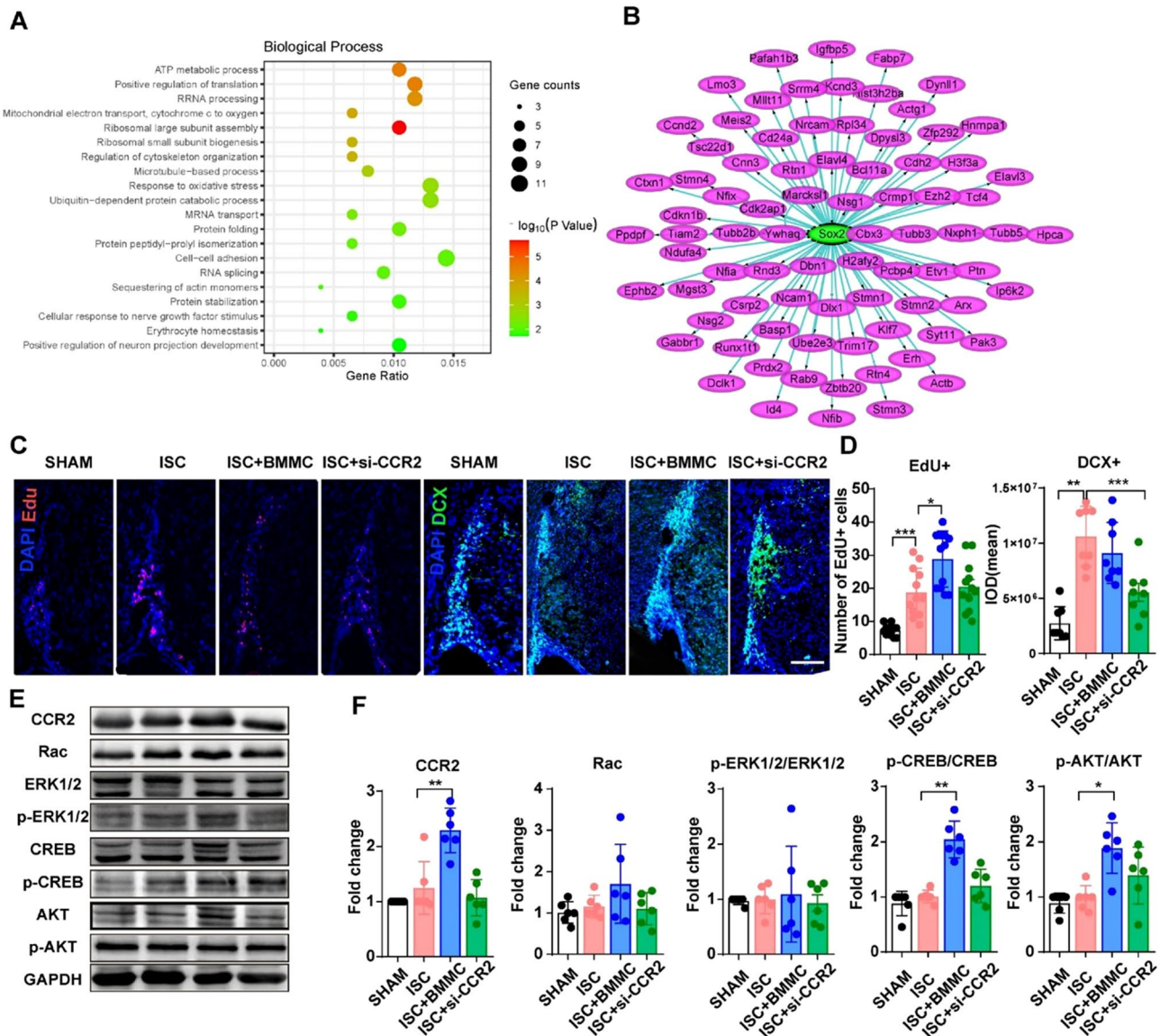


Fig. 6 Identifying regulators for neuronal regeneration after monocyte transplantation. **A** Bubble plots showing enrichment analysis of pseudo-dependent upregulated genes in the neural lineage (bubble size represents the gene counts in each enrichment term; color represents the $-\log_{10}(P \text{ value})$). **B** Regulon analysis of pseudo-dependent upregulated genes. Regulator SOX2 is located in the center and the arrows point to genes regulated by SOX2. **C**, **D** Representative

images and quantification of EdU+ and DCX+ cells in the SVZ. Data are the mean \pm SEM, $n = 8$ per group, scale bar = 100 μm . * $P < 0.05$; ** $P < 0.01$; *** $P < 0.001$. **E** Representative western-blot images of CCR2, Rac, ERK1/2, p-ERK1/2, Akt, p-Akt, CREB, p-CREB. **F** Analysis of Akt and CREB signaling at the protein level. Data are the mean \pm SEM, $n = 6$ per group. * $P < 0.05$; ** $P < 0.01$.

Discussion

Recent studies have demonstrated single-cell patterning and functional heterogeneity of brain myeloid cells under neuroinflammation, demyelination, and at different stages of neural development [10, 15]. However, single-cell mapping of brain myeloid cells under cerebral ischemic conditions at the chronic stage was still lacking. Similar to previous single-cell sequencing studies using peri-infarct

brain tissue in stroke models, we found that peri-infarct microglia were activated following cerebral ischemic injury, and their proportion was increased [24]. Multiple activation states of microglia rather than the classical M1 or M2 subtype were also found, along with downregulation of homeostatic markers like *Tmem119* and *Hexb*. In addition to these similarities, we revealed several novel findings. First, we identified two clusters of microglia associated with neurovascular plasticity, one with an expression

pattern similar to ATMs and the other characterized by upregulation of MAPK signaling genes. Marker genes of ATMs, including *Igf1* and *Spp1*, have been reported to be involved in the migration and neurogenesis of neuroblasts after stroke [21]. They also promote repair through phagocytosis [25]. Furthermore, Bioinformatics analysis of single-cell sequencing data, validated by immunofluorescence and flow cytometry, further revealed the interactions between bone marrow cells.

Bioinformatics analysis of single-cell sequencing data, validated by immunofluorescence and flow cytometry, further revealed the interactions between bone marrow cells. [11]. By single-cell differential expression analysis, we found an upregulation of genes favoring neurovascular plasticity and downregulation of deleterious neuroinflammatory responses in MDMs. Recent research [26] has suggested that the interaction between MDMs derived from the periphery and brain-resident microglia may mitigate the neural damage mediated by pro-inflammatory microglia. However, it remains unclear how infiltrating MDMs influence the polarization of microglia following cerebral ischemic injury. Our intercellular crosstalk predictions show that infiltrating MDMs displayed interactions with microglia *via* TGF β , Gas6, and Grn signaling, all of which are related to an anti-inflammatory and pro-repair phenotype of microglia [27, 28]. Microglia were also predicted to promote the proliferation and migration of neural cells through Sema-mediated direct contact with neural cells [29]. Furthermore, our flow cytometry results also demonstrated that infiltrated MDMs inhibited microglial proinflammatory responses and promoted post-stroke neurogenesis, consistent with a previous study showing that reduced proinflammatory microglia responses are associated with enhanced neurogenesis during stroke recovery [30]. However, the long-term interaction between BMDMs and microglia in the ischemic brain might also lead to excessive microglial activation and exacerbate neural damage [31]. Therefore, how the BMDM-microglia interaction regulates neuronal regeneration after ischemic injury needs to be revealed in future studies.

Consistent with neuronal developmental trajectories in the normal brain, genes associated with neuronal and axonal regeneration are upregulated in the significant trajectory progression of neuronal cells in the BMDC-ISC integration group [32]. However, near the central node, a subset of cells diverted into a branch related to immune responses, such as phagocytosis. Recent research [25] suggests that the interaction between MDMs derived from the periphery and brain-resident microglia may mitigate the neural damage mediated by pro-inflammatory microglia [33, 34]. Therefore, we interpreted this as a bidirectional trajectory where immature neuronal cells around

the infarct can either develop into mature neuronal cells or transform into debris-clearing neuronal cells.

Furthermore, our analysis suggested the repair-promoting effects of BMDM transplantation were mediated primarily by transcriptomic regulation of the transcription factor *Sox2*. *Sox2* has long been identified as a neurogenesis marker and a neurotrophic factor pathway regulator [35]. More importantly, microglia promote the proliferation of multi-potent stem cells in the spinal cord through a mechanism attributed to the MAPK-SOX2 signaling pathway [36]. The Sema pathway, identified in the analysis of microglia-neuronal cell interactions, also promotes neuronal repair through the activation of MAPK signaling [37]. Akt and CREB signaling are essential components of the neurotrophin and MAPK pathways. Moreover, Sema signaling, which our bioinformatics analysis predicted would mediate the interaction between microglia and neural cells, has been shown to be associated with the activation of Akt signaling [38]. As a result, we speculate that interactions between microglia and neural lineages after MDM transplantation might lead to improved neurogenesis through activation of Akt and CREB signaling and that the transcription factor *Sox2* plays a critical regulatory role in this process.

Acknowledgements We would like to thank the NHC Key Laboratory of Immunodermatology (China Medical University), the Key Laboratory of Immunodermatology, and the Ministry of Education (China Medical University) for providing experimental support. This work was supported by the National Natural Science Foundation of China (82071467), the International (Regional) Cooperation and Exchange Program of the National Natural Science Foundation of China (82111330075), the National Natural Science Foundation for Youth Scholars of China (81801053), the Innovation Team Support Plan of Universities in Liaoning Province (LT2019015), the Liaoning Provincial Key Research and Development Guidance Program (2019JH8/10300002), and the Liaoning Revitalization Talents Plan (XLYC1802097).

Conflict of interest The authors declare that the research was conducted in the absence of any commercial or financial relationships that could be construed as a potential conflict of interest.

Data Availability The datasets generated during and/or analyzed during the current study are available from the corresponding author upon reasonable request.

References

1. Kluge MG, Kracht L, Abdolhoseini M, Ong LK, Johnson SJ, Nilsson M. Impaired microglia process dynamics post-stroke are specific to sites of secondary neurodegeneration. *Glia* 2017, 65: 1885–1899.
2. Feng Y, Liao S, Wei C, Jia D, Wood K, Liu Q, *et al.* Infiltration and persistence of lymphocytes during late-stage cerebral ischemia in middle cerebral artery occlusion and photothrombotic stroke models. *J Neuroinflammation* 2017, 14: 248.
3. Eldahshan W, Fagan SC, Ergul A. Inflammation within the neurovascular unit: Focus on microglia for stroke injury and recovery. *Pharmacol Res* 2019, 147: 104349.

4. Fang W, Zhai X, Han D, Xiong X, Wang T, Zeng X, *et al.* CCR2-dependent monocytes/macrophages exacerbate acute brain injury but promote functional recovery after ischemic stroke in mice. *Theranostics* 2018, 8: 3530–3543.
5. Ito M, Komai K, Mise-Omata S, Iizuka-Koga M, Noguchi Y, Kondo T, *et al.* Brain regulatory T cells suppress astrogliosis and potentiate neurological recovery. *Nature* 2019, 565: 246–250.
6. Owens R, Grabert K, Davies CL, Alfieri A, Antel JP, Healy LM, *et al.* Divergent neuroinflammatory regulation of microglial TREM expression and involvement of NF- κ B. *Front Cell Neurosci* 2017, 11: 56.
7. Van Hove H, Martens L, Scheyltjens I, De Vlaminck K, Pombo Antunes AR, De Prijck S, *et al.* A single-cell atlas of mouse brain macrophages reveals unique transcriptional identities shaped by ontogeny and tissue environment. *Nat Neurosci* 2019, 22: 1021–1035.
8. Plemel JR, Stratton JA, Michaels NJ, Rawji KS, Zhang E, Sinha S, *et al.* Microglia response following acute demyelination is heterogeneous and limits infiltrating macrophage dispersion. *Sci Adv* 2020, 6: eaay6324.
9. Keren-Shaul H, Spinrad A, Weiner A, Matcovitch-Natan O, Dvir-Szternfeld R, Ulland TK, *et al.* A unique microglia type associated with restricting development of alzheimer's disease. *Cell* 2017, 169: 1276–1290.e17.
10. Jordão MJC, Sankowski R, Brendecke SM, Sagar Locatelli G, Tai YH, *et al.* Single-cell profiling identifies myeloid cell subsets with distinct fates during neuroinflammation. *Science* 2019, 363: eaat7554.
11. Wang R, Liu Y, Ye Q, Hassan SH, Zhao J, Li S, *et al.* RNA sequencing reveals novel macrophage transcriptome favoring neurovascular plasticity after ischemic stroke. *J Cereb Blood Flow Metab* 2020, 40: 720–738.
12. Zhao S, Zhao M, Xiao T, Jolkkonen J, Zhao C. Constraint-induced movement therapy overcomes the intrinsic axonal growth-inhibitory signals in stroke rats. *Stroke* 2013, 44: 1698–1705.
13. Satija R, Farrell JA, Gennert D, Schier AF, Regev A. Spatial reconstruction of single-cell gene expression data. *Nat Biotechnol* 2015, 33: 495–502.
14. Franzén O, Gan LM, Björkegren JLM. PanglaoDB: A web server for exploration of mouse and human single-cell RNA sequencing data. *Database (Oxford)* 2019, 2019: baz046.
15. Hammond TR, Dufort C, Dissing-Olesen L, Giera S, Young A, Wysoker A, *et al.* Single-cell RNA sequencing of microglia throughout the mouse lifespan and in the injured brain reveals complex cell-state changes. *Immunity* 2019, 50: 253–271.e6.
16. Kim EK, Choi EJ. Compromised MAPK signaling in human diseases: An update. *Arch Toxicol* 2015, 89: 867–882.
17. Qiu X, Mao Q, Tang Y, Wang L, Chawla R, Pliner HA, *et al.* Reversed graph embedding resolves complex single-cell trajectories. *Nat Methods* 2017, 14: 979–982.
18. Jin S, Guerrero-Juarez CF, Zhang L, Chang I, Ramos R, Kuan CH, *et al.* Inference and analysis of cell-cell communication using Cell Chat. *Nat Commun* 2021, 12: 1088.
19. Andrews WD, Barber M, Nemitz M, Memi F, Parnavelas JG. Semaphorin3A-neuropilin1 signalling is involved in the generation of cortical interneurons. *Brain Struct Funct* 2017, 222: 2217–2233.
20. Liu Z, An H, Song P, Wang D, Li S, Chen K, *et al.* Potential targets of TMEM176A in the growth of glioblastoma cells. *Onco Targets Ther* 2018, 11: 7763–7775.
21. Rogall R, Rabenstein M, Vay S, Bach A, Pikhovych A, Baermann J, *et al.* Bioluminescence imaging visualizes osteopontin-induced neurogenesis and neuroblast migration in the mouse brain after stroke. *Stem Cell Res Ther* 2018, 9: 182.
22. Janky R, Verfaillie A, Imrichová H, Van de Sande B, Standaert L, Christiaens V, *et al.* iRegulon: From a gene list to a gene regulatory network using large motif and track collections. *PLoS Comput Biol* 2014, 10: e1003731.
23. Cui CP, Zhang Y, Wang C, Yuan F, Li H, Yao Y, *et al.* Dynamic ubiquitylation of Sox2 regulates proteostasis and governs neural progenitor cell differentiation. *Nat Commun* 2018, 9: 4648.
24. Zheng K, Lin L, Jiang W, Chen L, Zhang X, Zhang Q, *et al.* Single-cell RNA-seq reveals the transcriptional landscape in ischemic stroke. *J Cereb Blood Flow Metab* 2022, 42: 56–73.
25. Kurisu K, Zheng Z, Kim JY, Shi J, Kanoke A, Liu J, *et al.* Triggering receptor expressed on myeloid cells-2 expression in the brain is required for maximal phagocytic activity and improved neurological outcomes following experimental stroke. *J Cereb Blood Flow Metab* 2019, 39: 1906–1918.
26. Greenhalgh AD, Zarruk JG, Healy LM, Baskar Jesudasan SJ, Jhelum P, Salmon CK, *et al.* Peripherally derived macrophages modulate microglial function to reduce inflammation after CNS injury. *PLoS Biol* 2018, 16: e2005264.
27. Gilchrist SE, Goudarzi S, Hafizi S. Gas6 inhibits toll-like receptor-mediated inflammatory pathways in mouse microglia *via* axl and mer. *Front Cell Neurosci* 2020, 14: 576650.
28. Yin F, Banerjee R, Thomas B, Zhou P, Qian L, Jia T, *et al.* Exaggerated inflammation, impaired host defense, and neuropathology in progranulin-deficient mice. *J Exp Med* 2010, 207: 117–128.
29. Deng S, Hirschberg A, Worzfeld T, Penachioni JY, Korostylev A, Swiercz JM, *et al.* Plexin-B2, but not plexin-B1, critically modulates neuronal migration and patterning of the developing nervous system *in vivo*. *J Neurosci* 2007, 27: 6333–6347.
30. Yu F, Huang T, Ran Y, Li D, Ye L, Tian G, *et al.* New insights into the roles of microglial regulation in brain plasticity-dependent stroke recovery. *Front Cell Neurosci* 2021, 15: 727899.
31. Werner Y, Mass E, Ashok Kumar P, Ulas T, Händler K, Horne A, *et al.* Cxcr4 distinguishes HSC-derived monocytes from microglia and reveals monocyte immune responses to experimental stroke. *Nat Neurosci* 2020, 23: 351–362.
32. Zywitza V, Misios A, Bunatyan L, Willnow TE, Rajewsky N. Single-cell transcriptomics characterizes cell types in the sub-ventricular zone and uncovers molecular defects impairing adult neurogenesis. *Cell Rep* 2018, 25: 2457–2469.e8.
33. Zhu Y, Crowley SC, Latimer AJ, Lewis GM, Nash R, Kucenas S. Migratory neural crest cells phagocytose dead cells in the developing nervous system. *Cell* 2019, 179: 74–89.e10.
34. Sailer MHM, Hazel TG, Panchision DM, Hoepfner DJ, Schwab ME, McKay RDG. BMP2 and FGF₂ cooperate to induce neural-crest-like fates from fetal and adult CNS stem cells. *J Cell Sci* 2005, 118: 5849–5860.
35. Mir S, Cai W, Carlson SW, Saatman KE, Andres DA. IGF-1 mediated neurogenesis involves a novel RIT1/Akt/Sox2 cascade. *Sci Rep* 2017, 7: 3283.
36. Ma Y, Deng M, Liu M. Effect of differently polarized macrophages on proliferation and differentiation of ependymal cells from adult spinal cord. *J Neurotrauma* 2019, 36: 2337–2347.
37. Wu H, Wang X, Liu S, Wu Y, Zhao T, Chen X, *et al.* Sema4C participates in myogenic differentiation *in vivo* and *in vitro* through the p38 MAPK pathway. *Eur J Cell Biol* 2007, 86: 331–344.
38. Smeester BA, Slipek NJ, Pomeroy EJ, Bomberger HE, Shamsan GA, Peterson JJ, *et al.* SEMA4C is a novel target to limit osteosarcoma growth, progression, and metastasis. *Oncogene* 2020, 39: 1049–1062.

Springer Nature or its licensor (e.g. a society or other partner) holds exclusive rights to this article under a publishing agreement with the author(s) or other rightsholder(s); author self-archiving of the accepted manuscript version of this article is solely governed by the terms of such publishing agreement and applicable law.